DOI: 10.1002/ejic.200600969

Synthesis and Optical Properties of β-BaB_2O_4 Network-Like Nanostructures

Qingrui Zhao,[a] Xi Zhu,[a] Xue Bai,[a] Haihua Fan,[b] and Yi Xie*[a]

Keywords: Nonlinear optics / Materials science / Sol–gel processes / Borates

Network-like nanostructures made from the nonlinear optical material beta barium metaborate (β-BaB_2O_4, β-BBO) have been successfully synthesized from a BBO gel precursor by a sol–gel method. The homogeneous BBO gel precursor is prepared by the hydrolysis and condensation of barium acetate, sorbitol, and boric acid in a mixture of polyethylene glycol (PEG200) and water. We have also demonstrated that the morphology of the synthesized β-BaB_2O_4 materials exerts a significant influence on the second harmonic generation (SHG) efficiency. Importantly, the preparation and second-order nonlinear optical studies with different shapes will offer great opportunities to explore the dependence of a material's second-order nonlinear optical properties on its morphology and is essential for the manufacture of potential nanoscale optoelectronic and nonlinear optical devices.

Introduction

Much attention has been focused on nonlinear optical (NLO) materials during the past decades owing to their promising future applications in a number of fields such as laser medicine, optical communication, and signal processing.[1–5] Among the nonlinear optical bulk crystals, beta barium metaborate (β-BaB_2O_4, β-BBO) has shown good promise due to its large second harmonic generation (SHG) coefficients. SHG is a well-documented nonlinear optical effect that occurs when laser radiation strikes the surface of a material and a fraction of the incident light is frequency-doubled.[6,7] Generally, β-BaB_2O_4 single crystals are prepared by high temperature solution growth, such as the Czochralski technique[8] and Flux method.[9] Recent developments in the fast evolving field of nanoscience and nanotechnology, where size and shape are crucial for the optoelectronic properties of materials, especially the preparation of various β-BBO nanostructures such as nanowires, nanorods, and nanotubes and studies on their SHG performance on the nanoscale, are worthy of note.[10,11] Most recently, Hong et al. have reported that β-BBO nanoparticles with a diameter of 40 nm,[12] which show promising applications in the photoelectronic industry, can be prepared by coprecipitation followed by annealing at 700 °C. Despite this excellent progress in our ability to prepare β-BBO nanoparticles, no reports concerning the synthesis of one-dimensional (1D) nanostructures are available as yet, which therefore limits the shape-and-size dependent nonlinear optical responses of this functional material.

1D Nanostructures are an ideal system not only for understanding the functional phenomena in low-dimensional systems but also for developing new generation nanodevices with high performance. Furthermore, it is generally accepted that 1D nanostructures provide a good system to investigate the relationship between size and properties.[11] However, as far as NLO materials are concerned, including $KNbO_3$, KH_2PO_4 (KDP), α-$LiIO_3$, and β-BBO etc., there are few reports on the synthesis of 1D nanostructures. Only recently, for example, have Magrez et al. reported the growth of $KNbO_3$ nanowires by a hydrothermal route.[13] Similarly, Pribošič et al. have recently prepared $KNbO_3$ perovskite in the form of nanoneedles and nanoplatelets by crystallization of the amorphous gel.[14] Further research efforts are therefore needed to develop the fabrication of 1D NLO nanostructures from only $KNbO_3$ to other NLO materials such as β-BBO.

Inspired by these ideas, in this paper we report a simple, inexpensive, and efficient sol–gel approach as the first example of a morphology-controlled synthesis of β-BaB_2O_4 nanostructures with novel and interesting 1D morphologies. Interestingly, we show that the prepared β-BaB_2O_4 nanorods self-organize to form network-like structures. β-BBO nanoparticles can also be fabricated by varying the experimental parameters. In addition, the second-harmonic generation (SHG) efficiency of β-BBO network-like nanostructures and nanoparticles are described. The experimental results indicate that the β-BBO network-like nanostructures and nanoparticles have obvious differences in their SHG efficiency, which suggests that SHG is sensitive to the electronic properties of nanostructures of varying shape, size,

[a] Nanomaterials and Nanochemistry, Hefei National Laboratory for Physical Sciences at Microscale, University of Science & Technology of China,
Hefei, Anhui 230026, P. R. China
[b] State Key Laboratory of Optoelectronic Materials and Technologies, Sun Yat-Sen University,
Guangzhou, 510275, China
Fax: +86-551-3603987
E-mail: yxie@ustc.edu.cn

composition, and spatial organization.[15–18] Thus, the preparation and properties of β-BBO nanostructures provide a fine example of the dependence of a material's second-order nonlinear optical properties on its morphology and will find many interesting applications in the field of NLO devices.

Results and Discussion

The crystal structure and phase composition of the as-prepared product were characterized by X-ray powder diffraction (XRD). Figure 1 (a) shows a typical XRD pattern of the as-prepared product. All the peaks can be readily indexed to the hexagonal phase of β-BBO (JCPDS file, no. 80-1489), with lattice constants of a = 12.53 and c = 12.72 Å (Figure 1, b). No characteristic peaks were observed for any impurities.

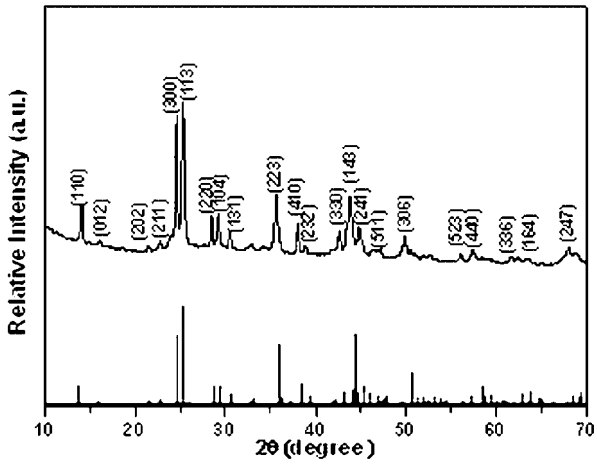

Figure 1. XRD pattern of network-like β-BaB_2O_4 nanostructures.

X-ray photoelectron spectra were also recorded to further characterize the product; the results are shown in Figure 2. High resolution spectra were recorded in the Ba 3d (Figure 2, a), B 1s (Figure 2, b), and O 1s (Figure 2, c) regions. The peak at 781.7 eV can be attributed to Ba $3d_{5/2}$, and the peak at 193.5 eV corresponds to B 1s of β-BaB_2O_4. The O 1s binding energy of 532.8 eV (Figure 2, c) indicates that the oxygen atoms are present as O^{2-} species in the compounds. These results are in good agreement with the values for crystalline β-BaB_2O_4 found in the literature.[19]

Further evidence for the composition of the sample was obtained from the Raman and IR spectra. The β-BBO crystal belongs to the C_{3v}^6 space group and group theory analysis predicts the zone–center optical modes A_1 and E, both of which are Raman and IR active. Figure 3 (a) shows the Raman spectra of a typical sample. The peaks centered at 1539, 784, 632, and 597 cm^{-1} can be assigned to A_1 [transversal-optical (TO) photon mode], and the peaks at 971, 661, 480, 384, and 703 cm^{-1} can be assigned to E [longitudinal-optical (LO) photon mode].[20] We also measured the IR spectra of the sample (Figure 3b). The full-range IR spectra between 800 and 3000 cm^{-1} shows broad absorptions in the range 900–1500 cm^{-1} for the characteristic absorption of β-BBO. The absorption peaks at 1078 and 1243 cm^{-1} are due to the B–O stretching modes in the BO_3^{3-}

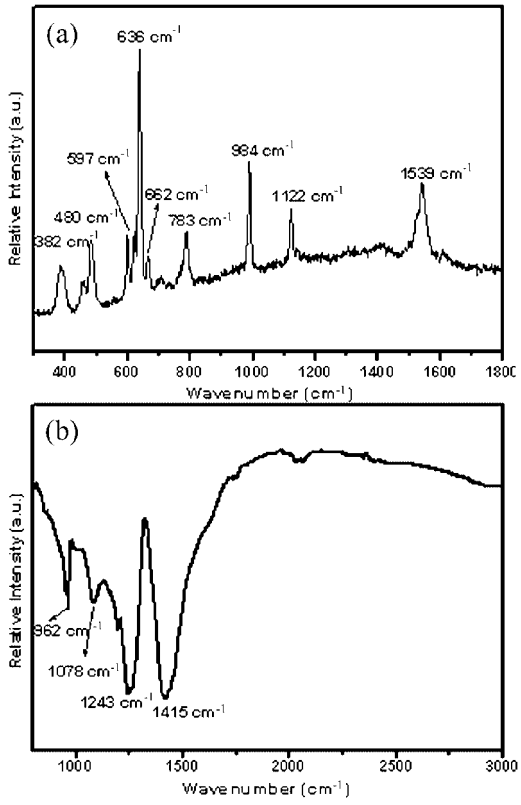

Figure 3. a) Raman and b) full-range IR spectra of the as-obtained β-BaB_2O_4 nanostructures.

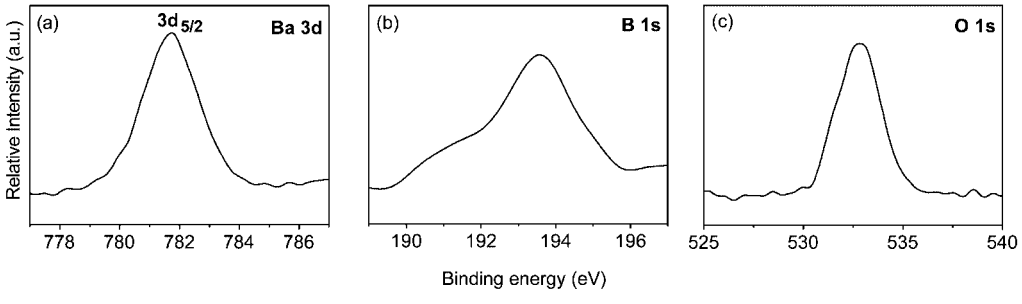

Figure 2. XPS spectra of network-like β-BaB_2O_4 nanostructures: a) high-resolution Ba region; b) high-resolution B region; c) high-resolution O region.

unit, which is a component of the $(B_3O_6)^{3-}$ ring.[21] The bands observed at 962 and 1415 cm^{-1} are B–O extra-ring stretching modes,[22] which is further evidence that high quality β-BBO nanocrystals have been obtained.

Figure 4 presents typical FESEM, TEM, and HRTEM images of the β-BBO network-like nanostructures obtained at different magnifications. The low magnification FESEM image in Figure 4 (a) shows the panoramic morphology of the products and the three-dimensional features and regularity of the network. Part b of Figure 4 is a TEM image, which reveals that the building blocks of the network-like nanostructures are uniform nanorods. These nanorods interlink in an orderly fashion that resembles a nanoweb. The average diameter of the nanorods is about 30 nm and their lengths range from 300 to 400 nm. Some building blocks of the network-like nanostructures are bundles of nanorods. For HRTEM imaging the samples were dispersed in ethanol and deposited on carbon-coated copper grids. The HRTEM image shown in parts c and d of Figure 4 show the high crystallinity of the product; defects such as twin structures, stacking faults, or dislocations are not seen in this image. This typical HRTEM image indicates that β-BBO nanostructures are single crystals that grow preferentially along the *a* [113] direction.

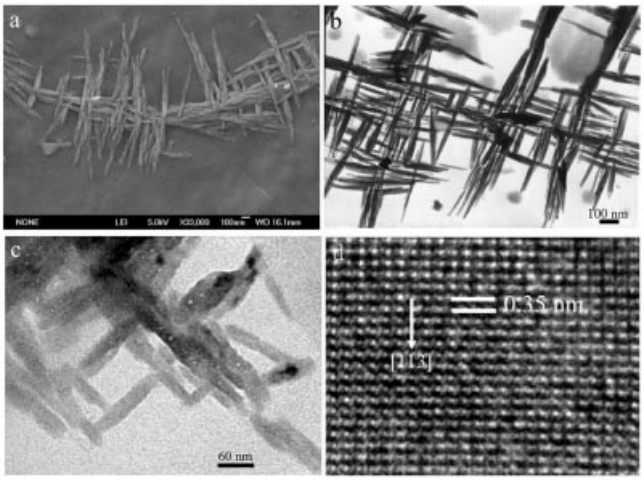

Figure 4. Electron microscopy images of the β-BaB_2O_4 network-like nanostructures: a) FESEM image; b) TEM image; c) high-magnification TEM image; d) HRTEM image along the [113] axis.

The sol–gel technique has been widely adopted to fabricate various nanostructures.[23] In our process, sorbitol coordinates to boric acid to form complexes by dehydration, which could prevent boric acid from volatilizing.[24] This complex solution then reacts with barium acetate, which loses its acetate to form the precursor.[25] When this mixture is heated continually it forms a homogeneous sol that then undergoes polycondensation and crosslinking to produce a gel. When calcined, this gel decomposes to form β-BBO nanostructures. The whole process is summarized in Scheme 1.

These β-BBO nanostructures are synthesized from a BBO gel precursor in a mixture of polyethylene glycol (PEG200) and water. The representative IR absorption

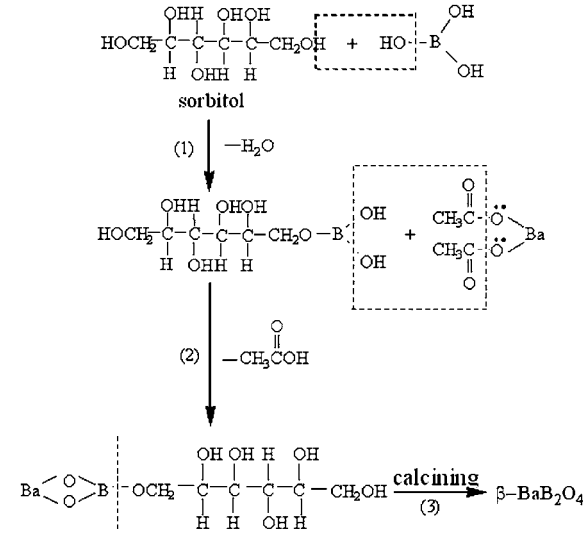

Scheme 1. The formation of β-BaB_2O_4.

spectra of the sol and gel shown in parts a and b of Figure 5 provide a direct way of investigating the sol–gel process. The bands at 2875, 1455, and 1351 cm^{-1} in part a of Figure 5 are assigned to the vibration of the C–H bond of PEG,[21] whereas the absorption peaks at 831, 888, and 944 cm^{-1} are due to the B–O stretching modes, which is a component of the $(B_3O_6)^{3-}$ ring.[21] The bands at 1100 and 1249 cm^{-1} are due to the vibration of the C–O bond,[26] and the intense bands at 1657 cm^{-1} are due to the presence of a carbonyl group.[27] Bands at around 1574, 1408, and 1069 cm^{-1} are clearly observed in Figure 5 (b). The strong absorption band from the carbonyl group at 1657 cm^{-1} has disappeared, which implies that acetic acid is released during the sol–gel process. The characteristic bands of PEG at 2875, 1455, and 1351 cm^{-1} have also disappeared, which indicates that the PEG has been removed completely. The appearance of a band at 1574 cm^{-1} indicates the presence of Ba–O. The absorption peak at 1069 cm^{-1} is due to the B–O stretching modes in the BO_3^{3-} unit and the band observed at 1408 cm^{-1} can be attributed to B–O extra-ring stretching modes.[21] The characteristic peaks of B–O at 1408 and 1069 cm^{-1} gradually shift to lower frequency and decrease in intensity, which suggests that polycondensation reactions of the H_3BO_3 precursor have occurred.

The cross-linking reagent PEG200 plays an important role in the formation of a gel precursor with high homogeneity, and hence a low degree of aggregation of the resulting nanostructures,[28] in this system, as can be seen from the IR spectra in Figure 5. The hydrolysis and polycondensation velocity of the precursor is lowered in the presence of PEG200, which minimizes the aggregation of the nanostructures during calcination. In addition, the short chain polymer PEG200 also acts as a structure-directing agent in the formation of 1D β-BBO nanostructures. PEG200 is easily adsorbed on the surface of the colloid due to its uniform and ordered chain structure, as reported previously.[29] From a kinetic point of view, if the polymer adsorbs on the surface of the growing colloid, thereby

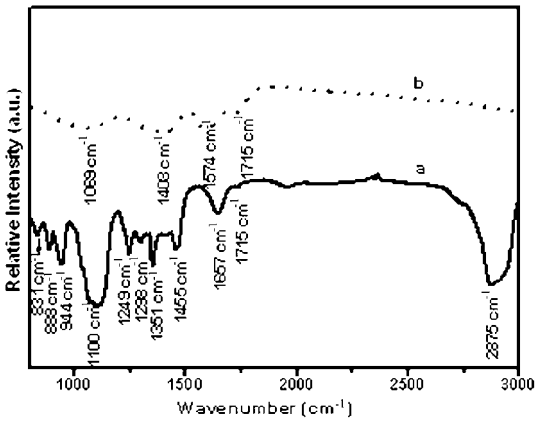

Figure 5. IR spectra of the samples in the sol–gel process: a) the precursor sol [$Ba(OAc)_2$ + H_3BO_3 + sorbitol + PEG); b) the precursor gel.

blocking this region, the growth of the colloid in one direction will be restricted. Therefore, the addition of PEG200 to the solution will modify the growth kinetics of the colloid, which finally leads to anisotropic growth of the samples. Previous research has provided many excellent samples where a polymer helps the growth of 1D nanostructures.[30] In the present work, PEG200 can efficiently adsorb to the surfaces of the precursor colloids, which leads to the growth of β-BBO along a certain direction.

We also performed a series of experiments to investigate the effect of the reaction conditions on the formation of β-BBO network-like nanostructures. We found that the use of PEG200 and the appropriate proportion of PEG200 and H_2O had a decisive effect on the formation of network-like β-BBO nanostructures. Our experiment showed that only β-BBO nanoparticles with an average diameter of 80 nm, as shown in Figure 6 (a), are formed in water with no PEG200, which confirms its important role as a structure-directing agent. When the experiment was carried out in the absence of water the reaction did not initiate and therefore no β-BBO was obtained. This result suggests that the addition of water increases the solubility of barium acetate, sorbitol, and boric acid and facilitates the formation of the homogeneous sol and the gel. The appropriate proportion of PEG200 is also critical for the formation of 1D β-BBO nanostructures. When the experiment was done with a PEG200 and H_2O ration 2:1 under otherwise identical conditions β-BBO shuttle-like nanostructures (Figure 6, b) were obtained. When the volume ratio of PEG200 and H_2O was changed to 1:1, however, β-BBO network-like nanostructures were obtained. This phenomenon might occur because the different amount of PEG200 results in a different rate of hydrolysis and condensation of the precursors.[31] The addition of an appropriate amount of PEG200 could control the rate of hydrolysis and condensation of the precursors and prevent the early precipitation of the metal ions from solution, thus allowing the formation of a homogeneous gel.

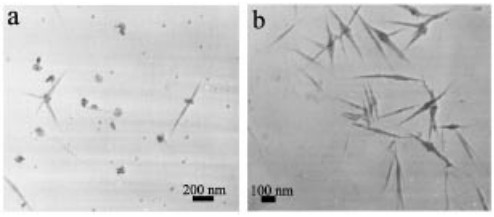

Figure 6. TEM images of as-prepared β-BaB_2O_4 samples formed in the presence of different amounts of PEG and H_2O: a) nanoparticles (without PEG); b) nanoshuttles (volume ratio of PEG and H_2O of 2:1).

It is known that β-BBO crystals have a high transmissivity from 190 to 3500 nm. Figure 7 (a) shows the UV/Vis/NIR absorption data of the as-obtained products. It can be seen that β-BBO is transparent up to 200 nm (6.22 eV). The absorption spectra are relatively featureless, and the broad and overall constant low absorbance from 200 to 1600 nm is consistent with the reported values for single crystals,[31] thus demonstrating that it is transparent from ultraviolet to the mid-infrared regions. The room temperature PL spectrum of the β-BBO network-like nanostructures (Figure 7, b) was recorded at an excitation wavelength of 245 nm. It can be seen that the spectrum features a strong emission band at 377 nm (approx. 3.3 eV). Earlier reports have indicated that β-BBO exhibits a dominant peak near 355 nm (3.5 eV).[32] The luminescence of these β-BBO network-like nanostructures at 3.3 eV is an intrinsic property of β-BBO due to radiative annihilation of the self-trapped exciton.[32]

Generally, NLO materials lacking an inversion symmetry and containing a π-electron conjugated system should exhibit an efficient SHG. Furthermore, SHG is sensitive to the electronic properties of nanostructures of varying shape, size, composition, and spatial organization. The structure of β-BBO (Scheme 2) is made up of slightly distorted $(B_3O_6)^{3-}$ anionic hexagonal groupings with a threefold axis. These plane-like $(B_3O_6)^{3-}$ units are stacked along the *c* axis.[33] The boroxyl ring $(B_3O_6)^{3-}$ is the unit that contributes most to the material's non-linearity.

Powder SHG measurements of the β-BBO network-like nanostructures (Figure 8) were performed to determine its second-order nonlinear optical behavior and hopefully allow us to determine the relationship between their properties and morphologies. The β-BBO nanostructures were irradiated with the fundamental laser wavelength of 1064 nm and light transmitted through the β-BBO nanostructures was found to have a wavelength of 531–533 nm, thus proving the generation of frequency doubling. The results in Figure 8 reveal that the SHG efficiency of the β-BBO network-like nanostructures is 78% relative to that of the reference sample (urea). At the same time, the contrast experiment found that the SHG efficiency of β-BBO nanostructures is nearly 10 times that of the β-BBO nanoparticles with a diameter of about 80 nm prepared without PEG200. These results indicate that the morphology of the materials has an important effect on their nonlinear optical properties and that the SHG is sensitive to the electronic properties of nanostructures of varying shape, size, composition,

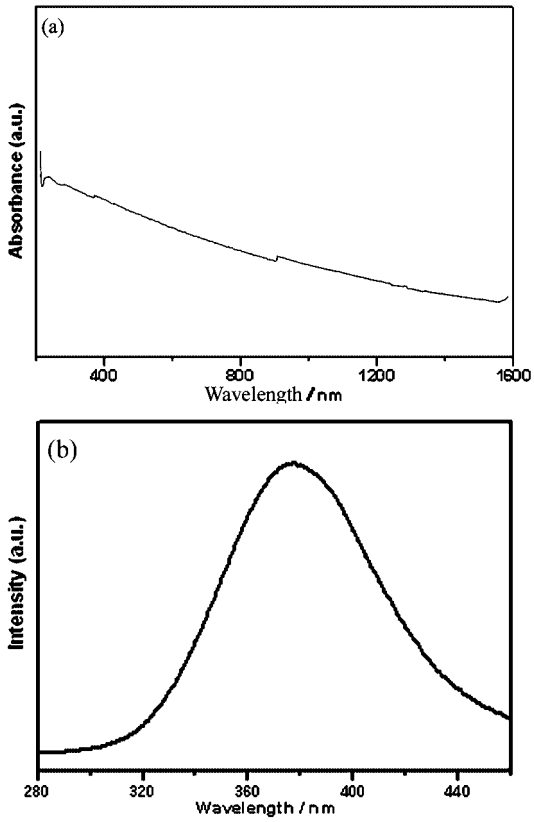

Figure 7. a) Absorption and b) PL spectra of β-BaB_2O_4 network-like nanostructures.

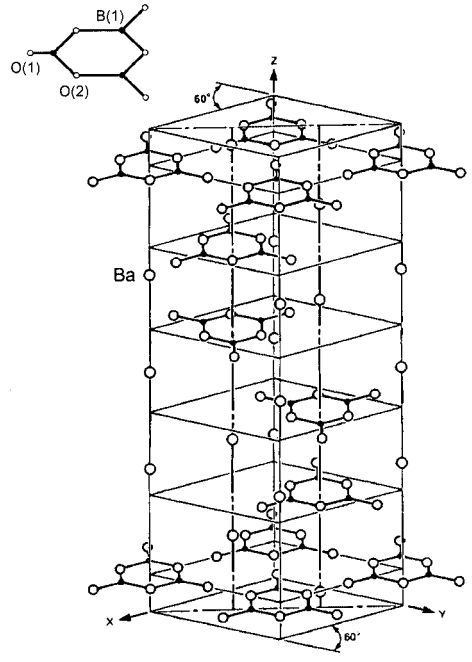

Scheme 2. Crystal structure of β-BaB_2O_4, which consists of nearly planar $(B_3O_6)^{3-}$ rings perpendicular to the polar axis that are bonded together through the barium atoms.

and spatial organization. For example, the measured second-order susceptibilities of ZnO nanowires are different from those of ZnO nanoribbons, which may be due to subtle changes in their structural or electronic properties.[34] This suggests that an in-depth investigation of the relationship between the structures and their second-order nonlinear optical susceptibilities is needed. Meanwhile, it is reasonable to suggest that some more complicated or special morphologies of β-BBO nanostructures with higher SHG intensity and wider transmissions might exist. This lays the groundwork for possible practical applications of nonlinear optical nanomaterials by replacing their single crystalline counterparts, and this kind of work on nonlinear optical nanomaterials provides new physical insights, which will be helpful to researchers in applied physics. Thus, there is still a long way to go in synthesizing nonlinear optical nanomaterials and studying their optical properties in the future.

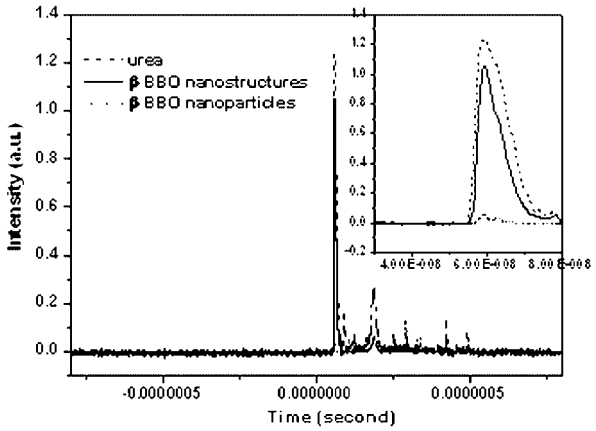

Figure 8. Powder SHG measurements of β-BaB_2O_4 network-like nanostructures, β-BaB_2O_4 nanoparticles, and reference sample urea. The inset is a high-magnification image.

Conclusions

In summary, a sol–gel method using the polymer PEG200 as structure-directing agent has been successfully used to synthesize β-BBO network-like nanostructures on a large scale. PEG200 plays an important role in the formation of β-BBO network-like nanostructures. This method has a lot of merits, such as not requiring complicated procedures and a short processing time. Investigations into the optical properties of β-BBO network-like nanostructures reveal that they have a wide transparency range from 200 to 1600 nm and a strong PL emission. The SHG efficiency of β-BBO nanostructures is close to that of urea and larger than that of β-BBO nanoparticles. Consequently, the fabrication and study of different β-BaB_2O_4 nanostructures has revealed the existence of a profound shape/property relationship and the potential promise for their application in the photoelectronics industry and as nonlinear optical devices.

Experimental Section

In a typical experiment, 6 mL of an aqueous solution containing barium acetate (0.25 g, 1 mmol), sorbitol (0.18 g, 1 mmol), and bo-

ric acid (0.13 g, 2 mmol) was put in a conical flask and stirred with a magnetic stirrer until a transparent solution had formed. This solution was then mixed with 6 mL of polyethylene glycol (PEG200, M_w = 200), in which the volume ratio of PEG200 and water was 1:1, and transferred into a 15-mL Teflon-lined stainless-steel autoclave. The mixed solution was kept at 180 °C for 12 h to homogenize the precursor sol. After the reaction was complete, the solution was heated to 330 °C for 5 h to form a homogeneous gel and then to 800 °C for 2 h under oxygen. The resultant white products were collected and rinsed several times with distilled water and absolute ethanol, and then dried under vacuum at 40 °C for 4 h.

The samples were characterized by X-ray powder diffraction (XRD) with a Japan Rigaku D/max rA X-ray diffractometer equipped with graphite-monochromated high-intensity Cu-K_α radiation (λ = 1.54178 Å) in the 2θ range from 10° to 70°. The transmission electron microscopy (TEM) images were recorded with a Hitachi Model H-800 instruments with a tungsten filament, using an accelerating voltage of 200 kV. The high-resolution transmission electron microscopy (HRTEM) images were recorded with a JEOL-2010 TEM at an acceleration voltage of 200 kV. The field emission scanning electron microscopy (FE-SEM) images were recorded with a JEOL JSM-6700F SEM. X-ray photoelectron spectroscopy (XPS) was performed with an ESCALAB MKII with Mg-K_α radiation (hv = 1253.6 eV) as the excitation source. The binding energies obtained in the XPS spectral analysis were corrected for specimen charging by referencing the C 1s peak to 284.6 eV. FT-IR absorption spectra were recorded with a Nicolet FT-IR-170SX spectrometer in the range 800–3000 cm^{-1} at room temperature, in transmission mode in a KBr pellet. Absorption spectra were recorded with a Shimadzu UV-365 UV/Vis-NIR Recording Spectrophotometer. The room-temperature photoluminescence (PL) spectra were recorded with a Jobin Yvon–Labram Steady-State/Lifetime Spectrofluorometer with an HeCd laser. The second-order nonlinear optical intensities were estimated for powder samples with a diameter of 76–154 μm in the form of a pellet. The thickness of each pellet was about 0.8 mm. The experimental arrangement for the nonlinear optical properties utilizes an OPG pumped by a PC2143 series laser at a repetition rate of 10 Hz. The selected wavelength is 1064 nm. After the selection of the wavelength, the laser beam is split into two parts, one of which is used to generate the second harmonic signal in the reference (urea pellet).

Acknowledgments

This work was financially supported by the National Nature Science Foundation of China (No. 20621061) and the State Key Project of Fundamental Research of Nanomaterials and Nanostructures (2005CB623601).

[1] L. F. Weaver, C. S. Petty, D. Eimerl, *J. Appl. Phys.* **1990**, *68*, 2589–2598.
[2] M. H. Dunn, M. Ebrahimzadeh, *Science* **1999**, *286*, 1513–1517.
[3] C. C. Chen, B. Wu, A. Jiang, G. You, *Science Sin. B* **1985**, *28*, 235–243.
[4] E. Delahaye, N. Tancrez, T. Yi, I. Ledoux, J. Zyss, S. Brasselet, R. Clément, *Chem. Phys. Lett.* **2006**, *429*, 533–537.
[5] T. Yi, R. Clément, C. Haut, L. Catala, T. Gacoin, N. Tancrez, I. Ledoux, J. Zyss, *Adv. Mater.* **2005**, *17*, 335–338.
[6] H. Nakatani, W. R. Bosenberg, L. K. Cheng, C. L. Tang, *Appl. Phys. Lett.* **1988**, *53*, 2587–2589.
[7] M. I. Stockman, D. J. Bergman, C. Anceau, S. Brasselet, J. Zyss, *Phys. Rev. Lett.* **2004**, *92*, 057402.
[8] H. Kouta, S. Imoto, Y. Kuwano, *J. Cryst. Growth* **1993**, *128*, 938–944.
[9] R. S. Feigelson, R. J. Raymeker, R. K. Route, *J. Cryst. Growth* **1989**, *97*, 352–366.
[10] J. Hu, T. W. Odom, C. M. Lieber, *Acc. Chem. Res.* **1999**, *32*, 435–445.
[11] Y. N. Xia, P. D. Yang, Y. G. Sun, Y. Y. Wu, B. Mayer, B. Gates, Y. D. Yin, F. Kim, H. Q. Yan, *Adv. Mater.* **2003**, *15*, 353–389.
[12] Y. F. Zhou, M. C. Hong, Y. Q. Xu, B. Q. Chen, C. Z. Chen, Y. S. Wang, *J. Cryst. Growth* **2005**, *276*, 478–484.
[13] A. Magrez, E. Vasco, J. W. Seo, C. Dieker, N. Setter, L. Forró, *J. Phys. Chem. B* **2006**, *110*, 58–61.
[14] I. Pribošič, D. Makovec, M. Drofenik, *Chem. Mater.* **2005**, *17*, 2953–2958.
[15] M. D. McMahon, R. Lopez, R. F. Haglund, *Phys. Rev. B* **2006**, *73*, 041401.
[16] R. C. Johnosn, J. T. Li, J. T. Hupp, G. C. Scatz, *Chem. Phys. Lett.* **2002**, *356*, 534–540.
[17] A. Podlipensky, J. Lange, G. Seifert, H. Graener, I. Cravetchi, *Opt. Lett.* **2003**, *28*, 716–718.
[18] E. C. Hao, G. C. Schatz, R. C. Johnson, J. T. Hupp, *J. Chem. Phys.* **2002**, *117*, 5963–5966.
[19] S. C. Sabharwal, S. K. Kulkarni, B. D. Padalia, *J. Mater. Sci.: Mater. Electronics* **2000**, *11*, 325–329.
[20] P. Ney, M. D. Fontana, K. Polgar, *J. Phys.: Condens. Networks* **1998**, *10*, 673–681.
[21] S. Hirano, T. Yogo, K. Kikuta, K. Yamagiwa, *J. Am. Ceram. Soc.* **1992**, *75*, 1697–1700.
[22] U. Moryc, W. S. Ptark, *J. Mol. Struct.* **1999**, *512*, 241–249.
[23] H. G. Yang, H. C. Zeng, *J. Phys. Chem. B* **2003**, *107*, 12244–12255.
[24] L. J. Q. Maria, M. I. B. Bernardi, A. R. Zanatta, A. C. Hernandes, V. R. Martelaro, *Mater. Sci. Eng. B* **2004**, *107*, 33–38.
[25] B. Guo, Z. L. Liu, L. Hong, H. X. Jiang, *Surf. Coat. Technol.* **2005**, *198*, 24–29.
[26] Y. Djaoued, P. V. Ashrit, S. Badilescu, R. Bruning, *J. Sol-Gel Sci. Technol.* **2003**, *28*, 235–244.
[27] G. Montanari, A. L. Costa, S. Albonetti, *J. Sol-Gel Sci. Technol.* **2005**, *36*, 203–211.
[28] H. L. Su, Y. Xie, P. Gao, Y. J. Xiong, Y. T. Qian, *J. Mater. Chem.* **2001**, *11*, 684–686.
[29] Z. Q. Li, Y. J. Xiong, Y. Xie, *Inorg. Chem.* **2003**, *42*, 8105–8109.
[30] Y. J. Xiong, Y. Xie, C. Z. Wu, J. Yang, Z. Q. Li, F. Xu, *Adv. Mater.* **2003**, *15*, 405–408.
[31] T. Yogo, K. Kikuta, K. Niwa, M. Ichida, A. Nakamura, S. Hirano, *J. Sol-Gel Sci. Technol.* **1997**, *9*, 201–209.
[32] I. N. Ogorodnikov, V. A. Pustovarov, A. V. Kruzhalov, L. I. Isaenko, M. Kirm, G. Zimmerer, *Phys. Solid State* **2000**, *42*, 1846–1853.
[33] D. Eimerl, L. Davis, S. Velsko, *J. Appl. Phys.* **1987**, *62*, 1968–1983.
[34] J. C. Johnson, K. P. Knutsen, H. Yan, M. Law, Y. F. Zhang, P. D. Yang, R. J. Saykally, *Nano. Lett.* **2004**, *4*, 197–204.

Received: October 15, 2006
Published Online: March 16, 2007

